Weyl semimetals, Fermi arcs and chiral anomalies

Shuang Jia, Su-Yang Xu and M. Zahid Hasan

Physicists have discovered a new topological phase of matter, the Weyl semimetal, whose surface features a non-closed Fermi surface whereas the low-energy quasiparticles in the bulk emerge as Weyl fermions. A brief review of these developments and perspectives on the next steps forward are presented.

Weyl semimetals are semimetals or metals whose quasiparticle excitation is the Weyl fermion, a particle that played a crucial role in quantum field theory but has not been observed as a fundamental particle in vacuum[1–24]. Weyl fermions have definite chiralities, either left-handed or right-handed. In a Weyl semimetal, the chirality can be understood as a topologically protected chiral charge. Weyl nodes of opposite chirality are separated in momentum space and are connected only through the crystal boundary by an exotic non-closed surface state, the Fermi arcs. Remarkably, Weyl fermions are robust while carrying currents, giving rise to exceptionally high mobilities. Their spins are locked to their momentum directions, owing to their character of momentum-space magnetic monopole configuration. Because of the chiral anomaly, the presence of parallel electric and magnetic fields can break the apparent conservation of the chiral charge, making a Weyl metal, unlike ordinary non-magnetic metals, more conductive with an increasing magnetic field. These new topological phenomena beyond topological insulators make new physics accessible and suggest potential applications, despite the early stage of the research[25–46].

In this Commentary, we will review key experimental progress and present an outlook for future directions of the field. We aim to expound our perspectives on the key results and the experimental approaches currently used to access the new physics, as well as their limitations. Moreover, although most of the current experiments focus on the discovery of new Weyl materials and demonstration of novel Weyl physics such as the chiral anomaly, it is becoming clear that a crucial step forward is to develop schemes for achieving quantum control of the new physics by electrical and optical means. We discuss some theoretical proposals along these lines, highlighting the experimental techniques and matching materials conditions that are necessary for realizing these research directions.

Topological material search

Although the theory of the Weyl semimetal has been around for a long time in various forms[1–4], its discovery had to wait until recent developments. This is because experimental realization requires appropriate simulation and characterizations of materials. Historically, the first two materials predicted to show the effect, the pyrochlore iridates $R_2Ir_2O_7$ (ref. 4) and the magnetically doped superlattice[6], were both time-reversal-breaking (magnetic) materials. Perhaps influenced by the early work, for a long while the community continued to focus on time-reversal-breaking materials as candidates for Weyl semimetals[7,10]. These candidates were extensively studied by many experimental groups. Unfortunately, their efforts were not successful in either demonstrating Fermi arcs or isolating the Weyl quasiparticles. Later, it was realized that the 'time-reversal-breaking' route to finding suitable materials faces a number of obstacles such as the strong correlations in magnetic materials, the destruction of sample quality upon magnetic doping, and the issue of magnetic domains in photoemission experiments.

On the other hand, for a long period, inversion-breaking Weyl materials were relatively unexplored. Following work on a semimetallic state located at a topological phase transition point[12], Singh and collaborators[13] discussed this possibility, but they considered compositional fine-tuning of spin–orbit strength in $TlBi(S_{1-x}Se_x)_2$, which is challenging to fabricate. Looking for Weyl semimetal candidates in naturally occurring inversion-breaking non-centrosymmetric single crystals can, however, avoid the difficulties described above. The advantages of this line of research for materials discovery were thoroughly discussed in ref. 14, where the search was based on the Inorganic Crystal Structure Database of FIZ Karlsruhe[27], which systematically records the lattice structure of crystals that have been synthesized over the course of a century. By following this approach and calculating the band structure of materials that are likely to be semimetals, many experimentally feasible Weyl semimetal candidates have been identified[10,14,28,29,34].

The theoretical prediction of Weyl semimetal states in the TaAs class of compounds was independently reported in 2015 by two groups[14,17]. The experimental realization of the first Weyl semimetal in TaAs followed soon after[15,18]. Both bulk Weyl cones and topological Fermi-arc surface states were directly reported by photoemission, providing a topological proof[15] based on methods shown earlier[16]. The negative magnetoresistance, which serves as an early signature of the chiral anomaly, was reported from transport experiments in the TaAs family of materials[19,20]. This family of materials was then experimentally shown to include NbAs and TaP (refs 10,21–24). A set of experimental criteria was developed for directly detecting topological Fermi arcs in Weyl semimetals without the need for detailed comparison with band-structure calculation[24]. At present, the TaAs family remain the only topological Weyl semimetals that have been clearly confirmed in experiments, independent of comparison to band-structure calculations[10,11].

The discovery of TaAs also established a feasible materials method to search for new Weyl semimetals that are more likely to be experimentally realizable. Shortly after TaAs, a number of new Weyl semimetal candidates along the same line of thinking were proposed.

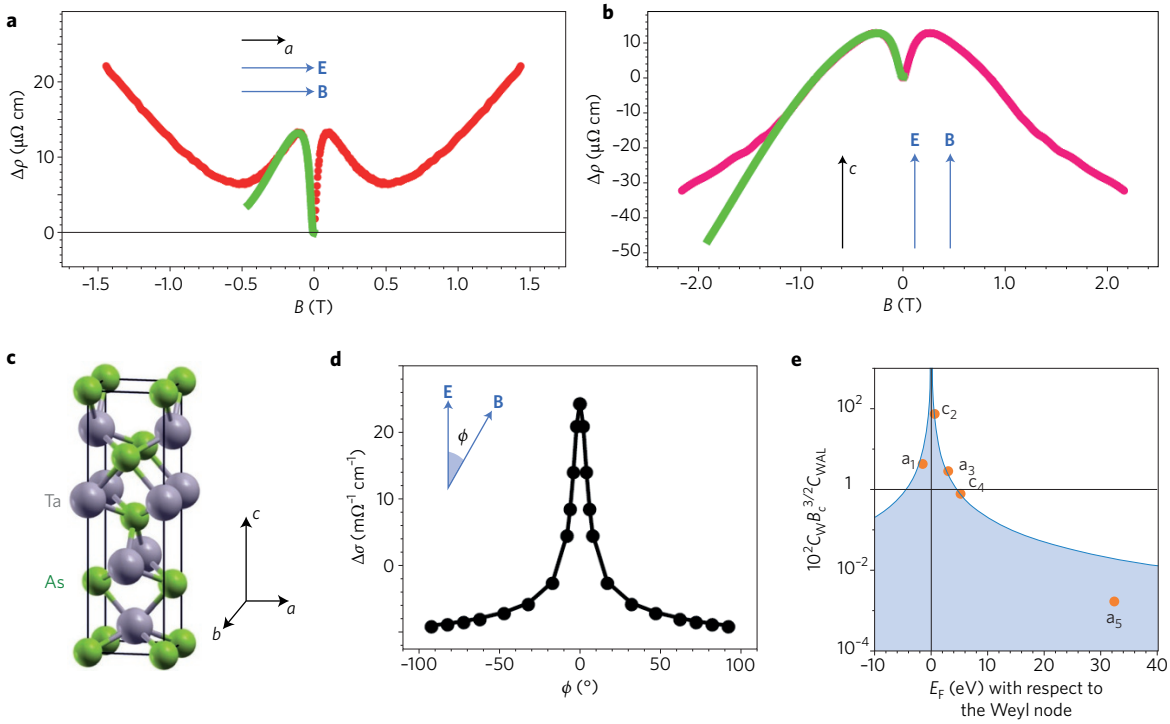

Figure 1 | Signatures of Adler–Bell–Jackiw chiral anomaly in TaAs. **a**,**b**, Longitudinal magnetoresistance data for TaAs. The red lines are the data, and the green lines are the theoretical fits. *a* and *c* are the lattice vectors along the in-plane and out-of-plane directions, respectively, of the TaAs tetragonal lattice. Background subtraction is discussed in ref. 20. **c**, The tetragonal crystal lattice of TaAs. **d**, Magnetoresistance data as a function of the angle between the electric (**E**) and magnetic (**B**) fields. **e**, Dependence of the chiral coefficient C_{WAL}, normalized by other fitting coefficients, on chemical potential, E_F. Remarkably, the observed scaling behaviour is $1/E_F^2$, as expected from the dependence of the Berry curvature on chemical potential in the simplest model of a Weyl semimetal, $\Omega \propto 1/E_F^2$. C_{WAL} is the coefficient describing the magnitude of the 3D weak anti-localization (WAL) effect. B_C is a critical field that characterizes a crossover between the WAL regime and the negative magnetoresistance regime. a_1, a_3, a_5, c_2 and c_4 are different samples measured in the experiments. These samples have slightly different chemical potential levels because they were grown under slightly different conditions. Adapted from ref. 20, Nature Publishing Group.

Primary examples include Ta_3S_2, $SrSi_2$, $Mo_{1-x}W_xTe_2$ and LaAlGe. In particular, $SrSi_2$ realizes a quadratic double Weyl state[29], while $Mo_{1-x}W_xTe_2$ (refs 30–33,35), LaAlGe (ref. 34) and Ta_3S_2 (ref. 28) are the 'type-II' Weyl semimetals, where the Weyl fermion manifests as a strongly Lorentz-violating, tilted-over cone in the band structure[30]. Experimental evidence of the bulk Weyl state has been shown in LaAlGe (ref. 34) and $Mo_{1-x}W_xTe_2$ (refs 35,36).

Transport response and chiral anomaly

Weyl fermions are expected to exhibit various forms of quantum anomalies such as a topological Fermi arc and chiral anomaly. The chiral anomaly is important in understanding some structures of the standard model of particle physics which is based on quantum field theory. A well-known case is the triangle anomaly associated with the decay of the neutral pion. Weyl semimetals provide an electronic route to realizing the chiral anomaly in condensed matter. Since the Weyl nodes are separated in momentum space, parallel magnetic and electric fields can pump electrons between Weyl nodes of opposite chirality that are separated in momentum space. This process violates the conservation of chiral charge and leads to an axial charge current, making a Weyl semimetal more conductive in an increasing magnetic field that is parallel to the electric field.

A clear identification of a Weyl semimetal with Fermi arcs in TaAs paved the way for the detection of the chiral anomaly. As shown in Fig. 1a,b, the magnetoresistance $\Delta\rho$ decreases with increasing magnetic field for a finite range of fields. The observed correct negative longitudinal magnetoresistance serves as an important first signature of the chiral anomaly. In addition, a number of supporting pieces of evidence were reported in ref. 20. These include the following. (1) There is a sharp dependence of the negative magnetoresistance on the angle between the electric and magnetic fields (Fig. 1d). (2) The presence of the negative magnetoresistance does not depend on the direction of the **E** field with respect to the crystalline axis. (3) The negative magnetoresistance shows a strong dependence on the chemical potential E_F. The chiral coefficient, which gives a measure of the magnitude of the chiral anomaly, diverges as the chemical potential approaches the energy of the Weyl node (Fig. 1e), consistent with its relation to the Berry curvature field. These transport results, in combination with angle-resolved photoemission spectroscopy (ARPES) data modelled to be consistent with them, demonstrated the existence of the chiral anomaly in TaAs driven by Weyl fermions. It is worth noting that the chiral anomaly can also arise in a Dirac semimetal because the Dirac fermions can split into pairs of Weyl fermions of opposite chirality under an external magnetic field[37].

In most metals, magnetoresistance is known to be positive; so a negative magnetoresistance, especially a longitudinal one, is quite rare. But the chiral anomaly is not the only possible origin. It may arise through the giant magnetoresistance effect in magnetic materials. Also, with a high electronic mobility, it can occur through a purely classical geometric effect, the current-jetting. Furthermore, the negative magnetoresistance due to the chiral anomaly is a Berry curvature effect. However, a generic band structure without Weyl nodes can carry non-zero Berry curvature

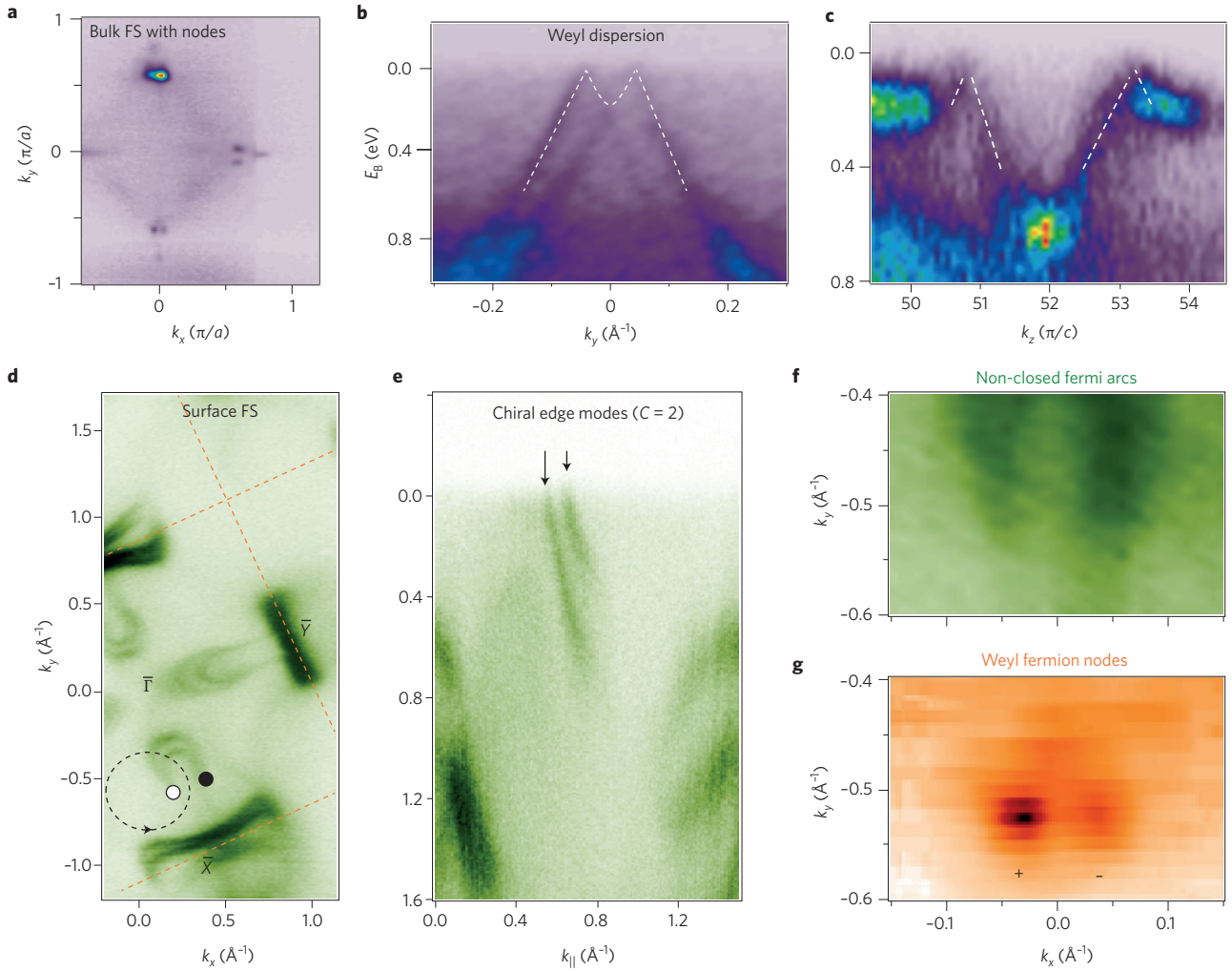

Figure 2 | Observation of Weyl fermions and topological Fermi arcs. **a**, ARPES-measured k_x, k_y bulk-band Fermi surface (FS) projection of TaAs. The Fermi surface consists of discrete 0D points that arise from the Weyl nodes. **b**, In-plane energy dispersion (E–k_y) that goes through a pair of Weyl nodes of opposite chirality. **c**, Out-of-plane energy dispersion (E–k_z) that goes through a pair of Weyl nodes. Panels **b** and **c** show that the bands disperse linearly away from the Weyl nodes along both the in-plane and the out-of-plane directions. **d**, Surface-state Fermi surface of TaAs. We focus on the crescent-shaped feature near the midpoint of the $\bar{\Gamma} - \bar{X}$ line. The Weyl semimetallic nature of TaAs can be demonstrated from the surface-state band structure as measured in ARPES by drawing a loop (dashed black line) in the surface Brillouin zone and counting the crossings to show a non-zero Chern number[15]. **e**, The surface states along the loop: two edge states of the same chirality seen in the momentum-space cuts of the ARPES data reveal a Chern number of 2 for this projection. ARPES methods for measuring Chern numbers are elaborated in refs 15,24,35. Note that for a conventional electron or hole pocket, such a counting argument should result in a null (0) value. **f**, Surface-state Fermi surface map at the k-space region corresponding to the terminations of the crescent Fermi arcs. **g**, Bulk Fermi surface map at the k-space region corresponding to the W2 Weyl nodes. Adapted from ref. 15, AAAS.

as long as time-reversal symmetry or inversion symmetry is broken. Whether such a generic band structure with non-zero Berry curvature yet without Weyl nodes can lead to a negative magnetoresistance is not theoretically understood. A recent experiment reported negative magnetoresistance in $ZrTe_5$ (ref. 38). There, the interpretation was that $ZrTe_5$ is a Dirac semimetal, and the Dirac fermion splits into pairs of Weyl fermions under the external magnetic effect. Subsequent photoemission and scanning tunnelling microscopy experiments[39,40] clearly revealed, however, that the robust electronic ground state of $ZrTe_5$ is that of a gapped semiconductor with a small (~50 meV) gap, not a Dirac semimetal. This suggests that a thorough theoretical understanding of the origins of the negative magnetoresistance in this material is lacking. Considering the complexity of the phenomenon, in order to achieve a convincing case, one needs to provide data that are sensitive to the unique properties of Weyl fermions and their systematic relation to the Berry curvature field. At present, only TaAs shows the dependence on the position of the chemical potential with respect to the energy of the Weyl node (see Fig. 1e) that systematically tunes the Berry curvature field effectively. Specifically, Fig. 1e shows that the magnitude of the chiral anomaly diverges over $1/E_F^2$. This demonstrates a Berry curvature monopole behaviour, and thus constitutes a strong signature of the topological Weyl fermion physics.

Weyl fermions and Fermi arc topology

ARPES serves as a decisive method of demonstrating the Weyl semimetal state experimentally, since it can directly observe bulk Weyl fermions and surface Fermi arcs in the electronic band structure, thus probing the bulk boundary correspondence

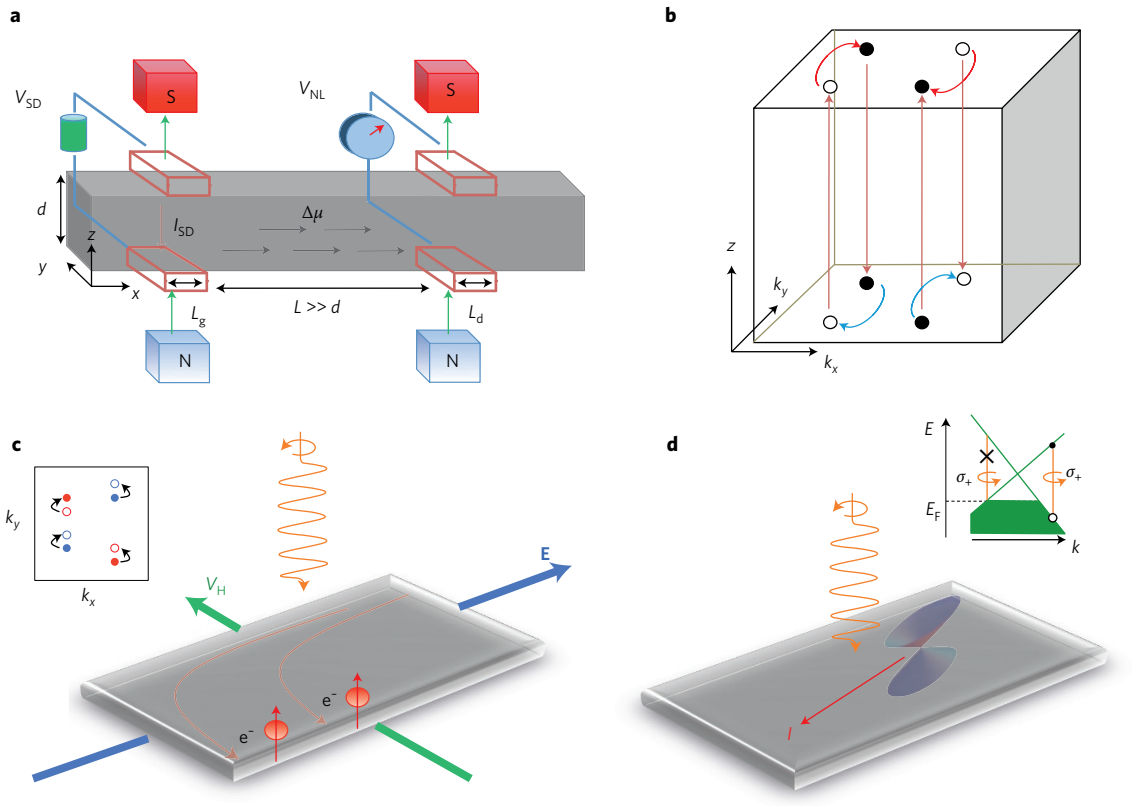

Figure 3 | Electronic and optical control of Weyl fermions. **a**, Schematics of a non-local electrical transport device that uses the axial current arising from the chiral anomaly. V_{NL}, non-local voltage; V_{SD}, source–drain voltage. **b**, On the surface of a Weyl semimetal, electrons exhibit an unusual path in real (z) and momentum ($k_x - k_y$) space under an external magnetic field along the z direction. Not all paths are shown in the figure. **c**, An intense circularly polarized light can break time-reversal symmetry and lead to a non-zero Hall conductivity through the Floquet effect in the absence of an external magnetic field. Inset: the solid (open) circles show the Weyl nodes in the absence (presence) of the light. **d**, Circularly polarized light can generate a large photogalvanic current in a Weyl semimetal that breaks inversion symmetry and any mirror symmetry. The inset shows the optical selection rule of right-handed circularly polarized light (σ_+) from the lower band to the upper band of the Weyl cone. Figure based on refs 41–43,45.

essential for proving a topological state of matter, as demonstrated for topological insulators[11,25,26]. Here we review key ARPES observations that led to an unambiguous bulk–boundary topological demonstration of the Weyl semimetal state in TaAs. This demonstration methodology is a useful guideline for future research in this field, as it can be more generally applied to discover Weyl or related topological states, or new topological quasiparticles in other materials.

A Weyl node is a crossing point between the bulk conduction and valence band. Thus detection of a Weyl node requires the ability to measure states along all three momentum-space directions, k_x, k_y and k_z. The k_z resolution is achieved by tuning different incident photon energies. The existence of bulk Weyl cones and Weyl nodes in TaAs is shown by the following experimental observations in Fig. 2a–c. (1) The bulk conduction and valence bands touch at zero-dimensional (0D) isolated points (Fig. 2a). (2) These two bands disperse linearly away from the crossing point along all three of k_x, k_y and k_z (Fig. 2b,c). (3) The band crossings are not located at a high-symmetry point or along a high-symmetry line but rather are observed at generic k points of the Brillouin zone (Fig. 2a–c). The surface Fermi arcs are demonstrated by the following key observations in the experimental data. (4) The ARPES-measured Fermi surface of TaAs (Fig. 2d) reveals a crescent-shaped feature consisting of two curves that join at their two end points. (5) The surface band structure along a k loop that encloses the end point of the crescent feature exhibits two chiral edge states, thus realizing a Chern number (C) of +2 (Fig. 2e), in analogy with the integer quantum Hall (IQH) chiral edge states. A Chern number is the band-structure invariant (momentum-space wavefunction winding index) that describes the topology of the IQH state. It counts the number of the protected edge states which is also proportional to the Hall conductivity. In contrast to the IQH case with a single protected edge state ($C = 1$), we now have two chiral edge states crossing the Fermi level, as seen in this momentum-space cut in the ARPES data (Fig. 2e). Therefore the Chern number is $C = 2$ (refs 15,24,35). This demonstrates that Weyl semimetals, in some aspects, feature momentum-space properties that are higher-dimensional analogues of quantum Hall-like states but without external magnetic fields[10]. An intrinsic IQH state is not possible in 3D (ref. 11). The observation of a non-zero Chern number in momentum space provides a clear and unambiguous demonstration of the topological origin of the Fermi arcs. The details of this Chern number method using ARPES are reported in refs 10,15,35,46. (6) Finally, ARPES data showed that the terminations of the Fermi arcs coincide with the projections of the Weyl nodes, demonstrating the topological correspondence principle between bulk and boundary (Fig. 2f,g) and therefore the materials' topologically non-trivial nature.

A few remarks are in order. The demonstration in TaAs only requires the above-described ARPES data along with established results in topological band

theory. It does not rely on an agreement between the details of band dispersions and first-principles band-structure calculations. Such an experimental demonstration of topological invariance is robust and reliable. By contrast, a number of recent ARPES works have attempted to prove the existence of topological Fermi arcs solely based on the agreement between ARPES data and surface band-structure calculations. Although an agreement does provide supporting evidence, it cannot serve as a proof of the Fermi arcs. These issues are detailed in refs 10,15. Finally, in general, the bulk Weyl fermions or the surface Fermi arcs are two sets of independent but equally sufficient evidence for the Weyl semimetal state. Observing one of them with sufficient details, without the other, is sufficient to demonstrate that a material is a type-I Weyl semimetal[24].

Quantum control of Weyl fermions

Superconductivity in Weyl materials can give rise to a new platform for realizing novel types of Majorana fermions, which is of great interest in quantum information science[8–11]. Although ARPES and magnetotransport established the experimental foundation of the Weyl semimetal state, they are primarily aimed at demonstrating the topological physics including Weyl fermions, topological Fermi arcs and the chiral anomaly.

For this frontier, we note that all Weyl semimetals discovered so far belong to the inversion-breaking class. Thus, finding a time-reversal-breaking (most likely magnetic) Weyl semimetal is an important future task. It is also of interest to find simpler materials with fewer Weyl points. Material searches are underway to find the 'hydrogen atom' versions of Weyl semimetals with the minimum number of Weyl points possible, either four Weyl nodes in inversion-breaking Weyl semimetals or two Weyl nodes in time-reversal-breaking Weyl semimetals and topological nodal-line fermion (new fermion) materials such as $PbTaSe_2$ (ref. 46).

Here, we highlight the potential application of Weyl semimetals in devices. It will be important to achieve systematic control over Weyl physics by electrical and optical means, so that these phenomena can potentially be harnessed in device settings.

A recent theoretical report[41] proposed an electrical device that can make use of current due to the chiral anomaly. The chiral charge pumping effect (Fig. 1f) leads to a current, the axial current, which is believed to be nearly dissipationless. Any relaxation of the axial current requires scattering from one Weyl node to the other, which occupies a limited volume of the parameter space as it involves a large specific momentum transfer vector that connects the two Weyl nodes. As shown in Fig. 3a, in this device it is proposed to have a thin and long ribbon of a Weyl semimetal sample. On the left, parallel magnetic and electric fields lead to the axial current, which can drift to the right and be detected in the form of a spontaneous voltage/current without applying an electric field. Another theoretical work[42] predicts a new type of quantum oscillation that arises from the topological Fermi arc surface states. As shown in Fig. 3b, a surface electron occupying a state on the Fermi arcs has to travel back and forth across the bulk of the sample in the presence of an out-of-plane magnetic field. A direct consequence is that the period of the oscillation as a function of inverse magnetic field $1/B$ now depends on the thickness of the sample. The proposed experiments not only provide transport demonstration of the chiral anomaly and the surface arcs independent of ARPES or the negative magnetoresistance, but also realize new device configurations that make use of the axial current and the Fermi arcs.

There have been a number of noteworthy theoretical proposals for achieving optical control of the new Weyl physics. For example, in a proposal for an optically induced anomalous Hall current in an inversion-breaking Weyl semimetal[43], the authors showed that an intense circularly polarized light can break time-reversal symmetry, which shifts the k-space location of the Weyl nodes through the Floquet effect[44], and therefore leads to a non-zero Hall conductivity in the absence of an external magnetic field (Fig. 3c). Another work[45] predicted a large photogalvanic current (as large as 10^7 A m^{-2} in TaAs) in inversion-breaking Weyl semimetals. The proposed photocurrent is due to the optical selection rules (Fig. 3d), and differs from the other proposal in that the current is induced only by shining light on the sample, without any additional external electric (or magnetic) field. The large photocurrent can be used for fabricating high-sensitivity and broad-bandwidth infrared detectors, and for light-harvesting schemes in solar cells.

But these are only guidelines for potential applications. The plethora of unusual physics harboured by Weyl materials may lead to something far more exotic that we have not yet imagined. ❐

Shuang Jia is at the International Center for Quantum Materials, School of Physics, Peking University and at the Collaborative Innovation Center of Quantum Matter, Beijing 100871, China. Su-Yang Xu is at the Laboratory for Topological Quantum Matter and Spectroscopy (B7), Department of Physics, Princeton University, New Jersey 08544, USA. M. Zahid Hasan is at the Laboratory for Topological Quantum Matter and Spectroscopy (B7), Department of Physics, Princeton University and at the Princeton Institute for Science and Technology of Materials (PRISM), Princeton, New Jersey 08544, USA.
e-mail: gwljiashuang@pku.edu.cn; mzhasan@princeton.edu

References

1. Weyl, H. *Z. Phys.* **56,** 330–352 (1929).
2. Herring, C. *Phys. Rev.* **52,** 365–373 (1937).
3. Murakami, S. *New J. Phys.* **9,** 356 (2007).
4. Wan, X., Turner, A. M., Vishwanath, A. & Savrasov, S. Y. *Phys. Rev. B* **83,** 205101 (2011).
5. Yang, K.-Y., Lu, Y.-M., Ran, Y. *Phys. Rev. B* **84,** 075129 (2011).
6. Burkov, A. A. & Balents, L. *Phys. Rev. Lett.* **107,** 127205 (2011).
7. Xu, G. *et al. Phys. Rev. Lett.* **107,** 186806 (2011).
8. Volovik, G. E. *The Universe in a Helium Droplet* (Oxford Univ. Press, 2009).
9. Ciudad, D. *Nat. Mater.* **14,** 863 (2015).
10. Hasan, M. Z., Xu, S.-Y., Belopolski, B. & Huang, S.-M. *Annu. Rev. Cond. Mat. Phys.* (in the press).
11. Hasan, M. Z., Xu, S.-Y. & Bian, G. *Phys. Scripta* **164,** 014001 (2015).
12. Xu, S.-Y. *et al. Science* **332,** 560–564 (2011).
13. Singh, B. *et al. Phys. Rev. B* **86,** 115208 (2012).
14. Huang, S. M., Xu, S.-Y. *et al. Nat. Commun.* **6,** 7373 (2015).
15. Xu, S.-Y. *et al. Science* **349,** 613–617 (2015).
16. Xu, S.-Y. *et al. Science* **347,** 294–298 (2015).
17. Weng, H. *et al. Phys. Rev. X* **5,** 011029 (2015).
18. Lv, B. Q. *et al. Phys. Rev. X* **5,** 031013 (2015).
19. Huang, X. *et al. Phys. Rev. X* **5,** 031023 (2015).
20. Zhang, C. *et al. Nat. Commun.* **7,** 10735 (2016).
21. Xu, S.-Y. *et al. Nat. Phys.* **11,** 748–754 (2015).
22. Liu, Z. *et al. Nat. Mater.* **15,** 27–31 (2016).
23. Lv, B. Q. *et al. Nat. Phys.* **11,** 724727 (2015).
24. Belopolski, I. *et al. Phys. Rev. Lett.* **116,** 066802 (2016).
25. Hasan, M. Z. & Kane, C. L. *Rev. Mod. Phys.* **82,** 3045–3067 (2010).
26. Hasan, M. Z. & Moore, J. E. *Annu. Rev. Cond. Mat. Phys.* **2,** 55 (2011).
27. ICSD; https://icsd.fiz-karlsruhe.de/search/basic.xhtml
28. Chang, G. *et al. Sci. Adv.* **2,** e1600295 (2016).
29. Huang, S.-M. *et al. Proc. Natl Acad. Sci. USA* **113,** 1180–1185 (2016).
30. Soluyanov, A. A. *et al. Nature* **527,** 495–498 (2015).
31. Sun, Y. *et al.* Preprint at http://arxiv.org/abs/1508.03501 (2015).
32. Chang, T.-R. *et al. Nat. Commun.* **7,** 10639 (2016).
33. Wang, Z. *et al. Phys. Rev. Lett.* **117,** 056805 (2016).
34. Xu, S.-Y. *et al.* Preprint at https://arxiv.org/abs/1603.07318 (2016).
35. Belopolski, I. *et al. Phys. Rev. B* **94,** 085127 (2016).
36. Huang, L. *et al. Nat. Mater.* http://dx.doi.org/10.1038/nmat4685 (2016).
37. Xiong, J. *et al. Science* **350,** 413–416 (2015).
38. Li, Q. *et al. Nat. Phys.* **12,** 550–554 (2016).
39. Wu, R. *et al. Phys. Rev. X* **6,** 021017 (2016).
40. Zhang, Y. *et al.* Preprint at http://arxiv.org/abs/1602.03576 (2016).
41. Parameswaran, S. A. *et al. Phys. Rev. X* **4,** 031035 (2014).
42. Potter, A. C. *et al. Nat. Commun.* **5,** 5161 (2014).
43. Chan, C.-K., Lee, P. A., Burch, K. S., Han, J. H. & Ran, Y. *Phys. Rev. Lett.* **116,** 026805 (2016).
44. Wang, Y.-H. *et al. Science* **342,** 453–457 (2013).
45. Chan, C.-K., Lindner, N. H., Refael, G. & Lee, P. A. Preprint at http://arxiv.org/abs/1607.07839 (2016).
46. Bian, G. *et al. Nat. Commun.* **7,** 10556 (2016).

Acknowledgements

We thank I. Belopolski, S.-M. Huang, G. Bian, N. Alidoust and M. Neupane for comments, and D. Haldane, I. Klebanov and E. Witten for discussion as a part of Princeton Summer School on New Insights Into Quantum Matter as a part of Prospects in Theoretical Physics Program at IAS. S.J. is supported by the National Basic Research Program of China (Grant No. 2014CB239302 and No. 2013CB921901). Work at Princeton by S.-Y.X and M.Z.H. is supported by the US Department of Energy under Basic Energy Sciences (Grant No. DOE/BES DE-FG-02-05ER46200 and No. DE-AC02-05CH11231 at Advanced Light Source at LBNL) and Princeton University funds. M.Z.H. acknowledges Visiting Scientist user support from Lawrence Berkeley National Laboratory, PRISM, and partial support from the Moore Foundation.